I&EC research
Industrial & Engineering Chemistry Research

pubs.acs.org/IECR

Article

Integrating Order-of-Magnitude Analysis to Physics-Informed Neural Networks for Linear Chromatographic Models

Yu-Cheng Chen, Shan-Jing Yao, and Dong-Qiang Lin*

Cite This: *Ind. Eng. Chem. Res.* 2025, 64, 3168−3182

Read Online

ACCESS | Metrics & More | Article Recommendations

ABSTRACT: A hybrid (gray-box) modeling framework, physics-informed neural networks (PINNs), has garnered significant attention. However, a huge challenge in applying PINNs to bioprocesses is developing a loss function that synergizes different bioprocess dynamics. To mitigate this challenge, a novel physics-based deep learning method was developed by integrating order-of-magnitude analysis to the loss function of PINNs (oPINNs) using biological first principles. Compared to standard PINNs and numerical methods for solving the forward problem of linear chromatographic models, oPINNs demonstrated notable improvements: an order-of-magnitude enhancement in accuracy with an equivalent sample size, or a 32-fold reduction in sample size for equivalent accuracy, along with a 1000-fold acceleration in computational speed for millisecond-scale simulation. Moreover, oPINNs showed exceptional robustness in weight determination and hyperparameter selection amidst variations in chromatographic model parameters. In summary, oPINNs represent a significant advancement in integrating physics-based deep learning into hybrid modeling of bioprocesses, particularly for developing real-time digital twins.

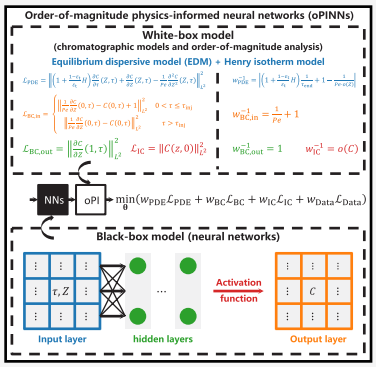

1. INTRODUCTION

The hybrid (gray-box) model, as a synergy of mechanistic (white-box) and data-driven (black-box) models, has emerged as an invaluable tool in bioprocess modeling.[1,2] This model leverages the first-principle understanding of bioprocesses accumulated over the past half-century while also utilizes flexible data-driven models to interpret the unidentifiable dynamics during bioprocesses.[3,4] This dual approach enhances robustness, improves extrapolation, and avoids overfitting.[5] Within this hybrid modeling framework, data-driven insights should complement mechanistic models—expressed through algebraic, ordinary differential, or partial differential equations (PDEs)—rather than replace them.[6,7] The degree of hybridization can quantify the contributions of white-box and black-box components in a hybrid model.[8,9] This complementary perfectly addresses a key challenge in bioprocess modeling: the lack of sufficient high-quality experimental data makes it difficult to establish fully data-driven models, while the unidentifiable dynamics may lead to overly simplified mechanistic models with poor fitting and predictability.[10−14]

Recently, a hybrid modeling framework known as physics-informed neural networks (PINNs) has garnered significant attention.[15−20] This approach integrates both PDEs and data into its loss function, utilizing the automatic differentiation properties of NNs for computing PDE losses.[21] PINNs are considered a promising hybrid modeling technique,[22−28] with potential applications extending from computational fluid dynamics in chemical processes to bioprocess modeling.[1,29−33]

However, research on PINNs in bioprocesses is still in its early stages, with applications currently limited to certain areas such as chromatography in bioseparations.[34−40] These studies emphasize a huge challenge: developing a loss function that synergizes different bioprocess dynamics. The development of this loss function is critical to the performance of PINNs, which have been even referred to as the "loss term method" by Thuerey et al.[41] Introducing weights into the loss function can help balance the influence of different loss terms. Current approaches for determining these weights in chromatography modeling include empirical fine-tuning,[35] cross-validation,[36,38−40] and adaptive adjustments.[34] While these methods can successfully train a PINN, they often prioritize empirical and mathematical aspects over underlying biological first-principles,[42] potentially undermining the integration of PINNs into bioprocess models. Therefore, there is an urgent need to develop a weight determination method based on first-principles to enhance this integration.

The concept of "weights" in the loss function refers to the assignment of different levels of importance to various loss terms. In chemical engineering, order-of-magnitude analysis

Received: October 7, 2024
Revised: January 10, 2025
Accepted: January 14, 2025
Published: January 29, 2025

https://doi.org/10.1021/acs.iecr.4c03744
Ind. Eng. Chem. Res. 2025, 64, 3168−3182

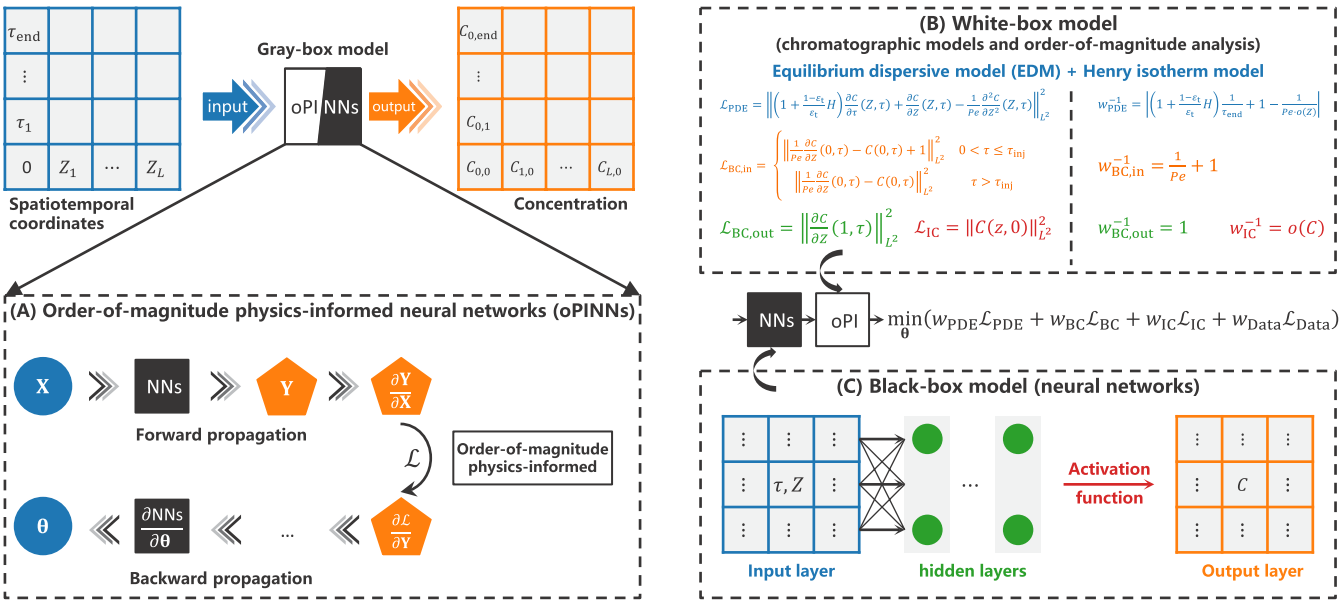

Figure 1. Schematic diagram of order-of-magnitude physics-informed neural networks (oPINNs). (A) forward and backward propagation of oPINNs. (B) white-box model including loss terms and the corresponding weights determined by order-of-magnitude analysis. (C) black-box model implemented by fully connected NNs.

serves as a powerful tool for assessing importance,[43,44] allowing engineers to estimate quantities to the nearest power of ten and quickly assess relative significance of different bioprocess dynamics. Consequently, the incorporation of order-of-magnitude analysis from chemical engineering into the loss function of PINNs has the potential to accelerate model training, facilitate convergence, enhance physical consistency, and reduce overfitting risks.

Once PINNs are reasonably trained, they can unlock a wide range of applications in bioprocesses, particularly those sensitive to computational efficiency.[1,45] Tang et al.[35] suggested that the significant speed improvements brought by PINNs hold promise for enabling real-time process control and the development of digital twins for chromatographic processes. Although analytical solutions exist for chromatographic models under ideal linear adsorption conditions in the Laplace domain,[46,47] practical nonlinear applications necessitate traditional grid-based numerical methods,[48−51] which often face a significant trade-off between computational cost and accuracy. Grid refinement can enhance solution accuracy but also demands more computational time. Consequently, numerical methods are often combined with reduced-order models or linearization techniques,[52] sacrificing some accuracy. In contrast, as a mesh-free approach, PINNs, can effectively eliminate this trade-off without any compromise. Previous studies[38,39] have applied PINNs to model-based process optimization, demonstrating a 250-fold reduction in computational time while maintaining accuracy comparable to traditional numerical methods.

To enhance the contribution of biological first-principles into the PINN loss function and address the computational cost-accuracy trade-off, this work introduces a novel approach that integrates order-of-magnitude analysis into PINNs (oPINNs). This generalized approach is specifically applied to linear chromatographic models (Section 2). The learning procedures for oPINNs are detailed in Section 3, while Section 4 evaluates the performance differences in accuracy, convergence, robustness, and computational efficiency between oPINNs and the reference methods (analytical solutions, numerical solutions, standard PINNs) in solving the forward problem of linear chromatographic models. Finally, Section 5 discusses the profound implications of oPINNs and their connection with calculus.

2. ORDER-OF-MAGNITUDE PHYSICS-INFORMED NEURAL NETWORKS

2.1. Physics-Informed Neural Networks. The solution y of chromatographic models includes the concentrations of the mobile phase c and the stationary phase q:

$$y(z, t) = [c(z, t) \quad q(z, t)]^{\mathrm{T}} \tag{1}$$

where z and t are axial position and time, respectively. The governing equation of eq 1 is

$$\frac{\partial y}{\partial t}(z, t) = [\frac{\partial c}{\partial t}(z, t) \quad \frac{\partial q}{\partial t}(z, t)]^{\mathrm{T}} \tag{2}$$

where $\frac{\partial c}{\partial t}$ and $\frac{\partial q}{\partial t}$ can be expressed by

$$\frac{\partial c}{\partial t}(z, t) = f(\frac{\partial c}{\partial z}, \frac{\partial^2 c}{\partial z^2}, \frac{\partial q}{\partial t}, z, t) \tag{3}$$

$$\frac{\partial q}{\partial t}(z, t) = g(c, q, z, t) \tag{4}$$

One can use a NN to approximate the solution y in eq 1. If the approximation y_h is sufficiently accurate, the PDEs in eqs 3 and 4 should naturally be satisfied. In other words, the PDE residual $\mathcal{L}_{\mathrm{PDE}}$ should be equal to zero:

$$\mathcal{L}_{\mathrm{PDE}} = \left\| \left[\frac{\partial c}{\partial t}(z, t) - f \ \frac{\partial q}{\partial t}(z, t) - g \right]^T \right\|_{L^2}^2 = 0 \tag{5}$$

where $\| \|_{L^2}^2$ denotes the L^2-norm. NNs can approximate y_h, thus the derivatives of NNs obtained using automatic differentiation can approximate the derivatives of y_h. f and g

https://doi.org/10.1021/acs.iecr.4c03744
Ind. Eng. Chem. Res. 2025, 64, 3168−3182

Table 1. Loss Terms and Corresponding Weights of oPINNs

term	loss $\mathcal{L}$	reciprocal of the weight w^{-1}
PDE	$\left\|\left(1+\frac{1-\varepsilon_t}{\varepsilon_t}H\right)\frac{\partial C}{\partial \tau}(Z,\tau)+\frac{\partial C}{\partial Z}(Z,\tau)-\frac{1}{\mathrm{Pe}}\frac{\partial^2 C}{\partial Z^2}(Z,\tau)\right\|_{L^2}^2$	$\left\|\left(1+\frac{1-\varepsilon_t}{\varepsilon_t}H\right)\frac{1}{\tau_{\mathrm{end}}}+1-\frac{1}{\mathrm{Pe}\cdot o(Z)}\right\|$
BC (inlet)	$\begin{cases}\left\|\frac{1}{\mathrm{Pe}}\frac{\partial C}{\partial Z}(0,\tau)-C(0,\tau)+1\right\|_{L^2}^2 & 0<\tau\le\tau_{\mathrm{inj}}\\ \left\|\frac{1}{\mathrm{Pe}}\frac{\partial C}{\partial Z}(0,\tau)-C(0,\tau)\right\|_{L^2}^2 & \tau>\tau_{\mathrm{inj}}\end{cases}$	$\frac{1}{\mathrm{Pe}}+1$
BC (outlet)	$\left\|\frac{\partial C}{\partial Z}(1,\tau)\right\|_{L^2}^2$	1
IC	$\left\|C(z,0)\right\|_{L^2}^2$	$o(C)$

in eq 5 can be determined using automatic differentiation and the expression of chromatographic models. To ensure the existence of a unique solution to the PDEs, loss terms $\mathcal{L}_{\mathrm{BC}}$ for boundary conditions (BCs) and $\mathcal{L}_{\mathrm{IC}}$ for initial conditions (ICs) must also be considered. Additionally, a data-driven loss term $\mathcal{L}_{\mathrm{Data}}$ is introduced to account for unidentifiable parts in the mechanistic models. As shown in Figure 1A, the solution of chromatographic models is reformulated into training a NN parametrized by $\boldsymbol{\theta}$ to minimize the loss function:

$$\min_{\theta}(\mathcal{L}_{\mathrm{PDE}}+\mathcal{L}_{\mathrm{BC}}+\mathcal{L}_{\mathrm{IC}}+\mathcal{L}_{\mathrm{Data}}) \tag{6}$$

This approach (PINNs) can approximate the solution to PDEs by training NNs via the integration of physics information. The loss function shown in eq 6 is unbiased and referred to as the unbiased PINNs in this study. Conversely, the biased PINNs includes weights:

$$\min_{\theta}(w_{\mathrm{PDE}}\mathcal{L}_{\mathrm{PDE}}+w_{\mathrm{BC}}\mathcal{L}_{\mathrm{BC}}+w_{\mathrm{IC}}\mathcal{L}_{\mathrm{IC}}+w_{\mathrm{Data}}\mathcal{L}_{\mathrm{Data}}) \tag{7}$$

Without any influence from observational data, $\mathcal{L}_{\mathrm{Data}}$, this optimization is defined as a forward problem, which involves obtaining for the model solution given all model parameters, essentially predicting the behavior of the system. Conversely, with the observed data or the model solution used, this optimization is named as an inverse problem. The inverse problem is fundamental in many applications, such as parameter estimation in modeling,[53] where the goal is to refine the model to accurately reflect real-world observations. In summary, while the forward problem is about prediction based on known parameters, the inverse problem seeks to deduce those parameters from known outcomes.

2.2. Linear Chromatographic Models. Equations 3 and 4 define a chromatographic model, which is specialized as the equilibrium dispersive model coupled with the linear isotherm. This model lumps all dispersion effects in only one parameter (apparent axial dispersion D_{app}) to describe band spreading for the mobile phase:

$$\frac{\partial c}{\partial t}(z,t)=-\frac{u}{\varepsilon_t}\frac{\partial c}{\partial z}(z,t)+D_{\mathrm{app}}\frac{\partial^2 c}{\partial z^2}(z,t)-\frac{1-\varepsilon_t}{\varepsilon_t}\frac{\partial q}{\partial t}(z,t) \tag{8}$$

where u and ε_t are superficial velocity and total porosity, respectively. The linear isotherm model with Henry coefficient H is considered for stationary phase:

$$q(z,t)=H\cdot c(z,t) \tag{9}$$

Combining eq 8 with 9 gives

$$\left(1+\frac{1-\varepsilon_t}{\varepsilon_t}H\right)\frac{\partial c}{\partial t}(z,t)=-\frac{u}{\varepsilon_t}\frac{\partial c}{\partial z}(z,t)+D_{\mathrm{app}}\frac{\partial^2 c}{\partial z^2}(z,t) \tag{10}$$

which is completed with Danckwerts BCs at the column inlet with an injection of a constant injection concentration c_{inj} for a given injection time t_{inj}:

$$-\frac{\varepsilon_t D_{\mathrm{app}}}{u_{\mathrm{col}}}\frac{\partial c}{\partial z}(0,t)+c(0,t)=\begin{cases}c_{\mathrm{inj}} & 0<t\le t_{\mathrm{inj}}\\ 0 & t>t_{\mathrm{inj}}\end{cases} \tag{11}$$

and Neumann BCs at column outlet

$$\frac{\partial c}{\partial z}(L,t)=0 \tag{12}$$

A fully regenerated column is considered as ICs:

$$c(z,0)=0 \tag{13}$$

2.3. Dimensionless Models. To eliminate dimensional differences of physical quantities in the chromatographic models and reduce the number of parameters, it is necessary to transform governing equations, BCs, and ICs into dimensionless forms. The dimensionless variables for mobile phase concentration, stationary phase concentration, axial position, and time are defined as

$$C=c/c_{\mathrm{inj}} \tag{14}$$

$$Q=q/c_{\mathrm{inj}} \tag{15}$$

$$Z=z/L \tag{16}$$

$$\tau=\frac{ut}{\varepsilon_t L} \tag{17}$$

The ratio of convective transport to axial dispersion is defined by the axial Péclet number:

$$\mathrm{Pe}=\frac{uL}{\varepsilon_t D_{\mathrm{app}}} \tag{18}$$

Substituting eqs 14, 15, 16, 17, and 18 into eq 10 yields the following dimensionless mass balances:

$$\left(1+\frac{1-\varepsilon_t}{\varepsilon_t}H\right)\frac{\partial C}{\partial \tau}(Z,\tau)=-\frac{\partial C}{\partial Z}(Z,\tau)+\frac{1}{\mathrm{Pe}}\frac{\partial^2 C}{\partial Z^2}(Z,\tau) \tag{19}$$

https://doi.org/10.1021/acs.iecr.4c03744
Ind. Eng. Chem. Res. 2025, 64, 3168−3182

$$-\frac{1}{\mathrm{Pe}}\frac{\partial C}{\partial Z}(0,\tau)+C(0,\tau)=\begin{cases}1 & 0<\tau\le\tau_{\mathrm{inj}}\\ 0 & \tau>\tau_{\mathrm{inj}}\end{cases} \tag{20}$$

$$\frac{\partial C}{\partial Z}(1,\tau)=0 \tag{21}$$

$$C(z,0)=0 \tag{22}$$

The loss terms based on eqs 19, 20, 21, and 22 are detailed in Table 1.

2.4. Order-of-Magnitude Analysis. Based on order-of-magnitude analysis, we proposed a novel approach to determine the weights of PINNs, termed as oPINNs. Specifically, four weights need to be determined: w_{PDE}, $w_{\mathrm{BC,in}}$, $w_{\mathrm{BC,out}}$, and w_{IC}. The objective of weight determination in oPINNs is to scale different loss terms to a consistent magnitude, thereby preventing dominance by any single loss term and reducing the dimensionality of hyperparameter search. We estimate the magnitude of each loss term through order-of-magnitude analysis and utilize the reciprocal of these estimates as their respective weights to achieve consistent magnitudes and the equalization of different loss terms. We denote the approximate scaling of a physical quantity with the symbol "∼".

For a fully regenerated column, eq 22, it follows that $C = 0$. While oPINNs simulate C approaching zero, exact $C = 0$ cannot be achieved, resulting in a residual termed infinitesimal $o(C)$. This defines the dimensionality of the IC in eq 22:

$$C\sim o(C) \tag{23}$$

Consequently, the weight for the IC is determined as

$$w_{\mathrm{IC}}^{-1}=o(C) \tag{24}$$

Similar to the infinitesimal of concentration, one can define infinitesimals $o(\tau)$ for time and $o(Z)$ for length, sequentially obtaining the dimensionality of each term in eq 19:

$$\frac{\partial C}{\partial \tau}\sim\frac{o(C)}{o(\tau)}=\frac{1}{\tau_{\mathrm{end}}} \tag{25}$$

$$\frac{\partial C}{\partial Z}\sim\frac{o(C)}{o(Z)}=1 \tag{26}$$

$$\frac{\partial^2 C}{\partial Z^2}\sim\frac{o(C)}{o^2(Z)}=\frac{1}{o(Z)} \tag{27}$$

Therefore, the weight for the PDE is determined as

$$w_{\mathrm{PDE}}^{-1}=\left|\left(1+\frac{1-\varepsilon_t}{\varepsilon_t}H\right)\frac{1}{\tau_{\mathrm{end}}}+1-\frac{1}{\mathrm{Pe}\cdot o(Z)}\right| \tag{28}$$

The dimensionality of each term for the column inlet BC in eq 20 is

$$\frac{\partial C}{\partial Z}(0,\tau)\sim\frac{o(C)}{o(Z)}=1 \tag{29}$$

If $0<\tau\le\tau_{\mathrm{inj}}$,

$$-C(0,\tau)+1\sim -o(C)+1\sim 1 \tag{30}$$

If $\tau>\tau_{\mathrm{inj}}$,

$$C(0,\tau)\sim 1 \tag{31}$$

Accordingly, the weight for the column inlet BC is

$$w_{\mathrm{BC,in}}^{-1}=\frac{1}{\mathrm{Pe}}+1 \tag{32}$$

The dimensionality of the column outlet BC in eq 21 is

$$\frac{\partial C}{\partial Z}(1,\tau)\sim\frac{o(C)}{o(Z)}=1 \tag{33}$$

Thus, the weight for the column outlet BC is

$$w_{\mathrm{BC,out}}^{-1}=1 \tag{34}$$

The loss terms and corresponding weights of oPINNs are listed in Table 1 and Figure 1B.

3. METHODS AND MATERIALS

3.1. Analytical and Numerical Solution. This study evaluated the performance of the proposed oPINNs for solving the linear chromatographic models, based on comparisons between oPINNs, standard unbiased PINNs, analytical solutions, and traditional numerical methods.

The chromatographic models, composed of eqs 19, 20, 21, and 22, are second-order nonhomogeneous linear differential equations with constant coefficients. Its analytical solution can be obtained through the Laplace transform and its inverse, with specific expressions referenced from Van Genuchten[46] and Qamar et al.[47]

The chromatographic models can also be solved using numerical methods. A high-order accurate numerical method (DG-FEM) has demonstrated excellent performance in solving chromatographic models.[54−56] Fluxes for both the convection and diffusion terms used central fluxes, which ensures that for odd-order polynomials, the order of convergence matches the polynomial order.

3.2. Forward Problem. In this work, $\mathcal{L}_{\mathrm{Data}}$ in eq 7 was ignored, so we focused on solving the forward problem of linear chromatographic models. This problem involves the governing equation in eq 19, BCs in eqs 20 and (21), and IC in eq 22, with three model parameters: $\frac{1-\varepsilon_t}{\varepsilon_t}H$, Pe, and τ_{inj}. The dimensionless $\frac{1-\varepsilon_t}{\varepsilon_t}H$ and Pe were provided by the numerical experiments of Chen et al.[57] and Chen et al.:[58]

$$\frac{1-\varepsilon_t}{\varepsilon_t}H=\frac{1-0.58}{0.58}\times 0.20\times\left[\frac{0.57}{(0.55+0.05)/2}\right]^{7.00}\approx 13 \tag{35}$$

$$\mathrm{Pe}=\frac{0.278\times 250.00}{0.58\times 0.21}\approx 571 \tag{36}$$

Assuming a total simulation time $\tau_{\mathrm{end}} = 20$, τ_{inj} was set to 2 and 20 to simulate two classical conditions in chromatography experiments: pulse injection and breakthrough experiments.

3.3. Model Implementation in Pytorch. A fully connected NN was used to develop the proposed oPINNs. This network (Figure 1C) comprised two input nodes (Z and τ), one output node (C), n_{L} hidden layers, and n_{l} nodes per layer, with each linear layer followed by an activation function. The training loss was calculated by the mean squared error (MSE) and minimized by the Adam and L-BFGS optimizers. The gradient information required for the loss calculation was obtained through PyTorch's automatic differentiation feature.

https://doi.org/10.1021/acs.iecr.4c03744
Ind. Eng. Chem. Res. 2025, 64, 3168−3182

Table 2. Search spaces and optimums of hyperparameters under consideration

Hyperparameter	Symbol	Search space	Optimum
number of hidden layers	n_L	{1,2,3,4,5,6}	4
number of nodes per layer	n_l	{4,8,16,32,64,128,256}	64
learning rate	-	$\{10^{-2},10^{-3},10^{-4}\}$	10^{-3}
activation function	-	{sigmoid, tanh, ReLU}[a]	tanh
infinitesimal[b]	$o(Z)/o(C)$	$\{10^{-1},10^{-2},10^{-3},10^{-4}\}$	10^{-3}

[a]The linear layer initialization for different activation functions follows PyTorch's defaults. [b]$o(Z)/o(C)$ is a hyperparameter investigated specifically for oPINNs.

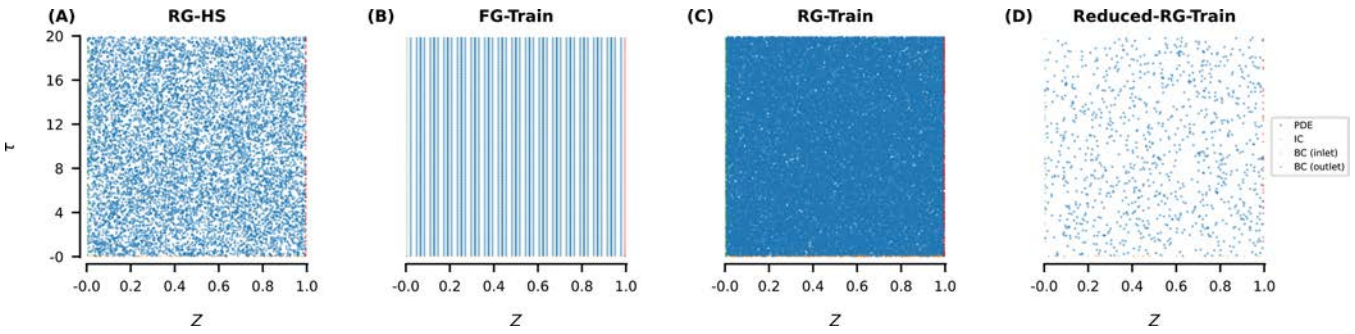

Figure 2. Two-dimensional spatiotemporal grids of RG and FG. (A) 10300 RG sample points for hyperparameter search. (B) 64640 FG sample points, with a polynomial order of 3 and 16 elements for model training. (C) 65278 RG sample points for model training. (D) 2050 reduced RG sample points for model training. For RG sample points, the ratio of PDEs, ICs, and BCs is n_{mesh}^2: n_{mesh}: $2n_{mesh}$ where n_{mesh} is the side length of the grid.

For a fair comparison, all four solutions (oPINNs, standard PINNs, DG-FEM, and the analytical solution) involved in this work were implemented using PyTorch's double-precision floating-point tensors.[59] All computations were executed on an Intel i9−13900K CPU with GPU acceleration provided by an RTX 4080. The time integration in DG-FEM was performed using the backward differentiation formula (BDF).

3.4. Hyperparameter Selection. Before the formal performance evaluation of the methods, we selected hyperparameters for oPINNs and PINN using a grid search approach[60] with the Adam and L-BFGS optimizers for 1000 and 500 epochs, respectively, which constitutes 5% of the formal training epochs. The sample sizes were fixed: 100 × 100 for PDEs, 100 for ICs, and 2 × 100 for BCs. Uniform random sampling was employed, and a fixed random seed ensured that the linear layers had the same initialization. The hyperparameters under consideration fell into five categories, with their search spaces detailed in Table 2. The total number of hyperparameter searches was 3024 for oPINNs and 1008 for PINN. We selected and fixed the appropriate hyperparameters for the subsequent parts of our research.

3.5. Evaluation of Accuracy and Convergence. Accuracy and convergence of three approximation methods (oPINNs, standard PINNs, and DG-FEM) were evaluated in solving the forward problem of linear chromatographic models, using the analytical solution as the benchmark. Both oPINNs and standard PINNs were trained under optimal hyperparameters, with training conducted using the Adam and L-BFGS optimizers for 20000 and 10000 epochs, respectively. Training was stopped early if the change in the loss function is less than 10^{-6} or if the relative change is less than 10^{-3}. These tolerance parameters were consistent with those used for the BDF method in DG-FEM solution.

The accuracy was evaluated by calculating MSE. To distinguish this from the training error, we referred to it as the evaluating error. The accuracy of oPINNs and standard PINNs was influenced by the sampling of spatiotemporal coordinates. Two sampling methods were examined in Figure 2: one where the mesh generated by DG-FEM served as the sample points for PINNs, referred to as the FEM-generated (FG) mesh; and another where uniform random sampling was used, referred to as the random-generated (RG) mesh. The total number of sample points for RG mesh was constrained to fractions of the DG-FEM mesh density: 1/1, 1/2, 1/4, 1/8, 1/16, 1/32, 1/64. The accuracy of DG-FEM was affected by the order, number of elements, and integration step size. Since DG-FEM was a high-order method, we set the order to 3. The examined number of elements are {4,8,16}, with the BDF integration step size fixed at 1‰ of the total simulation time.

For convergence evaluation, DG-FEM examined the ability of the numerical solution to progressively approach the exact solution as the mesh was refined. For oPINNs and standard PINNs, besides investigating the effect of mesh refinement, the convergence of the loss function during training was also examined.

3.6. Evaluation of Robustness. Weights in our proposed oPINNs include two model parameters, $\frac{1-\varepsilon_t}{\varepsilon_t}H$ and Pe, as shown in eqs 28 and 32, respectively. $\frac{1-\varepsilon_t}{\varepsilon_t}H$ is an adsorption isotherm parameter that couples the column total porosity with the elution behavior. Pe, on the other hand, is a mass transfer parameter, defined as the ratio of the convection rate to axial dispersion.

To investigate the effect of these two parameters on oPINNs and to evaluate the robustness of oPINNs under their variation, these two parameters were varied to 8, 4, 2, 1/2, 1/4, and 1/8 times their original values and 1/2, 1/4, 1/8, 1/16, 1/32, and 1/64 times their original values, respectively. This variation was determined based on their physical significance.[61] Then, the performance of the oPINNs under these conditions was assessed and compared to that of

https://doi.org/10.1021/acs.iecr.4c03744
Ind. Eng. Chem. Res. 2025, 64, 3168−3182

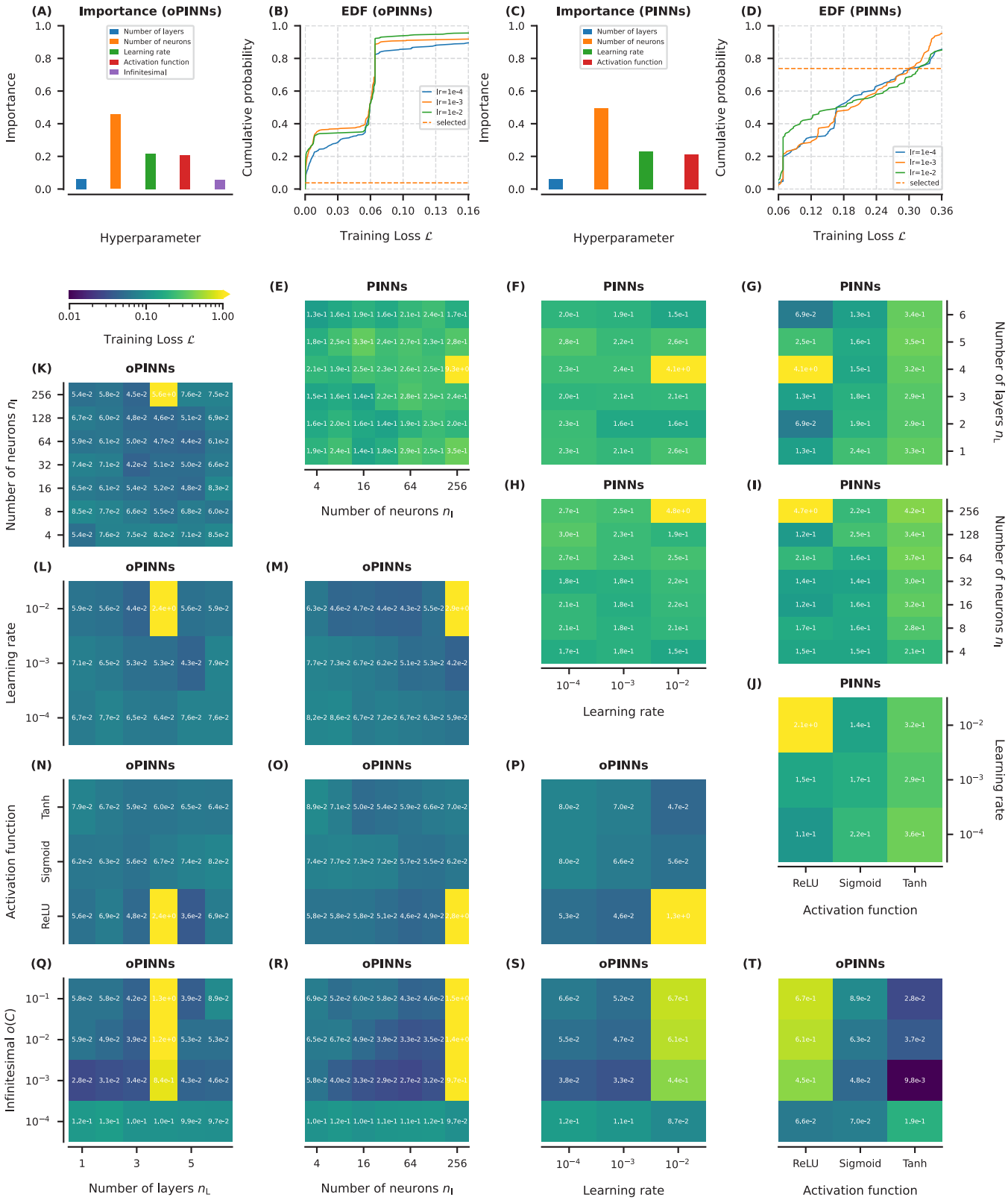

Figure 3. Pulse-injection experiments: hyperparameter importance using oPINNs (A) and PINNs (C), empirical distribution function using oPINNs (B) and PINNs (D), results of hyperparameter selection using PINNs (E-J) and oPINNs (K-T).

standard PINNs and DG-FEM. This evaluation includes examining the robustness of the method for determining the weights and hyperparameters in oPINNs.

For comparison, the DG-FEM was set to a polynomial order of 3 with 4 elements. Both oPINNs and standard PINNs utilized random sampling, with the total number of sample points kept consistent with the mesh density of the DG-FEM.

3.7. Evaluation of Computational Efficiency. The computational efficiency of oPINNs and DG-FEM was evaluated under varying sample sizes (grid densities) for the

https://doi.org/10.1021/acs.iecr.4c03744
Ind. Eng. Chem. Res. 2025, 64, 3168−3182

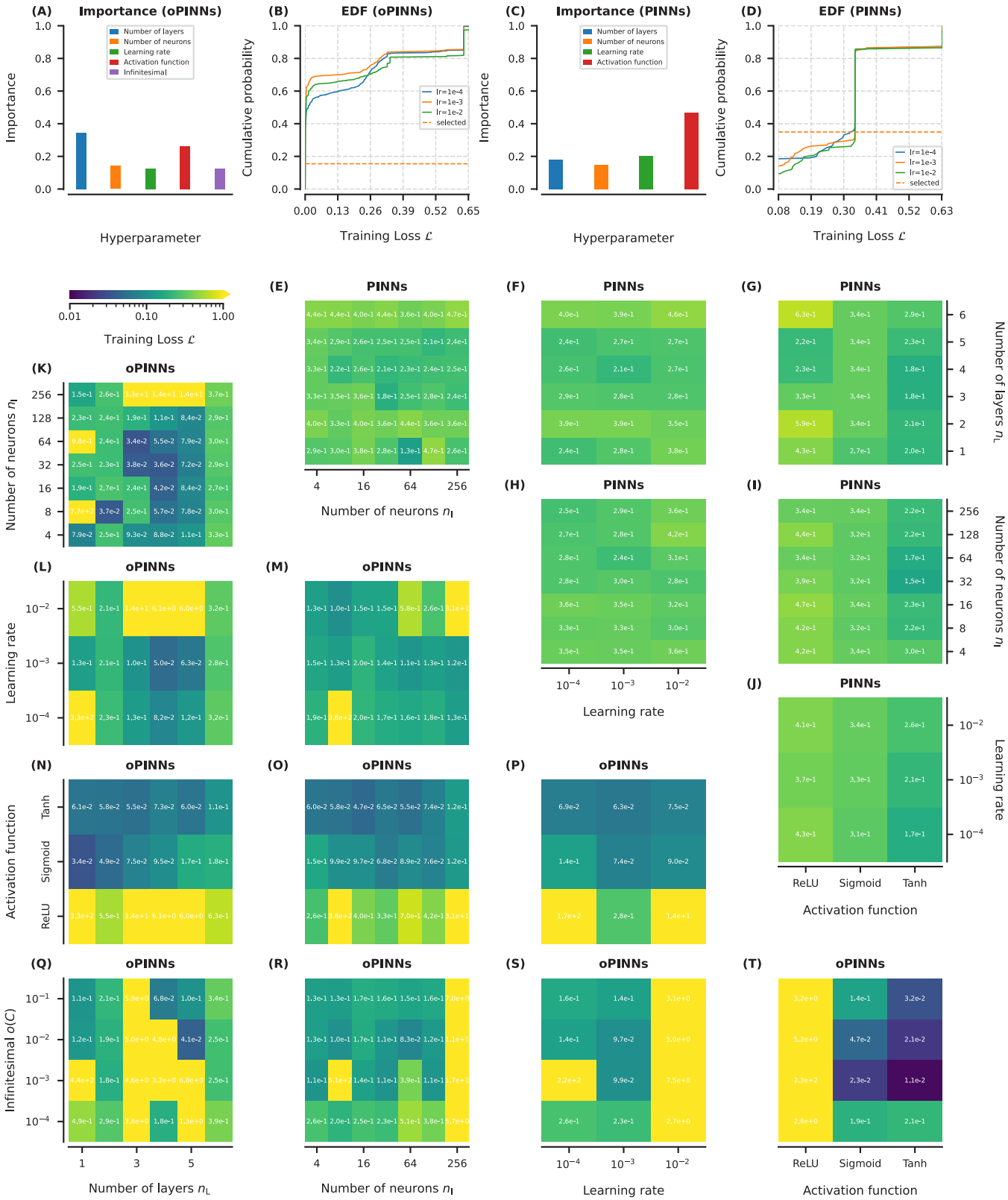

Figure 4. Breakthrough experiments: hyperparameter importance using oPINNs (A) and PINNs (C), empirical distribution function using oPINNs (B) and PINNs (D), results of hyperparameter selection using PINNs (E–J) and oPINNs (K–T).

forward problem of linear chromatographic models. To ensure a fair comparison, we implemented the DG-FEM code using PyTorch's tensors and obtained the Jacobian matrix using PyTorch's automatic differentiation. For oPINNs, the cost time per iteration during training was recorded. Similar to the accuracy evaluation, the computational efficiency of oPINNs was assessed using both FG and RG meshes. All computations were GPU-accelerated, with a single 6.00 GHz CPU core activated. The time cost was measured using the *timeit* magic command in Jupyter Notebook, which automatically deter-

https://doi.org/10.1021/acs.iecr.4c03744
Ind. Eng. Chem. Res. 2025, 64, 3168−3182

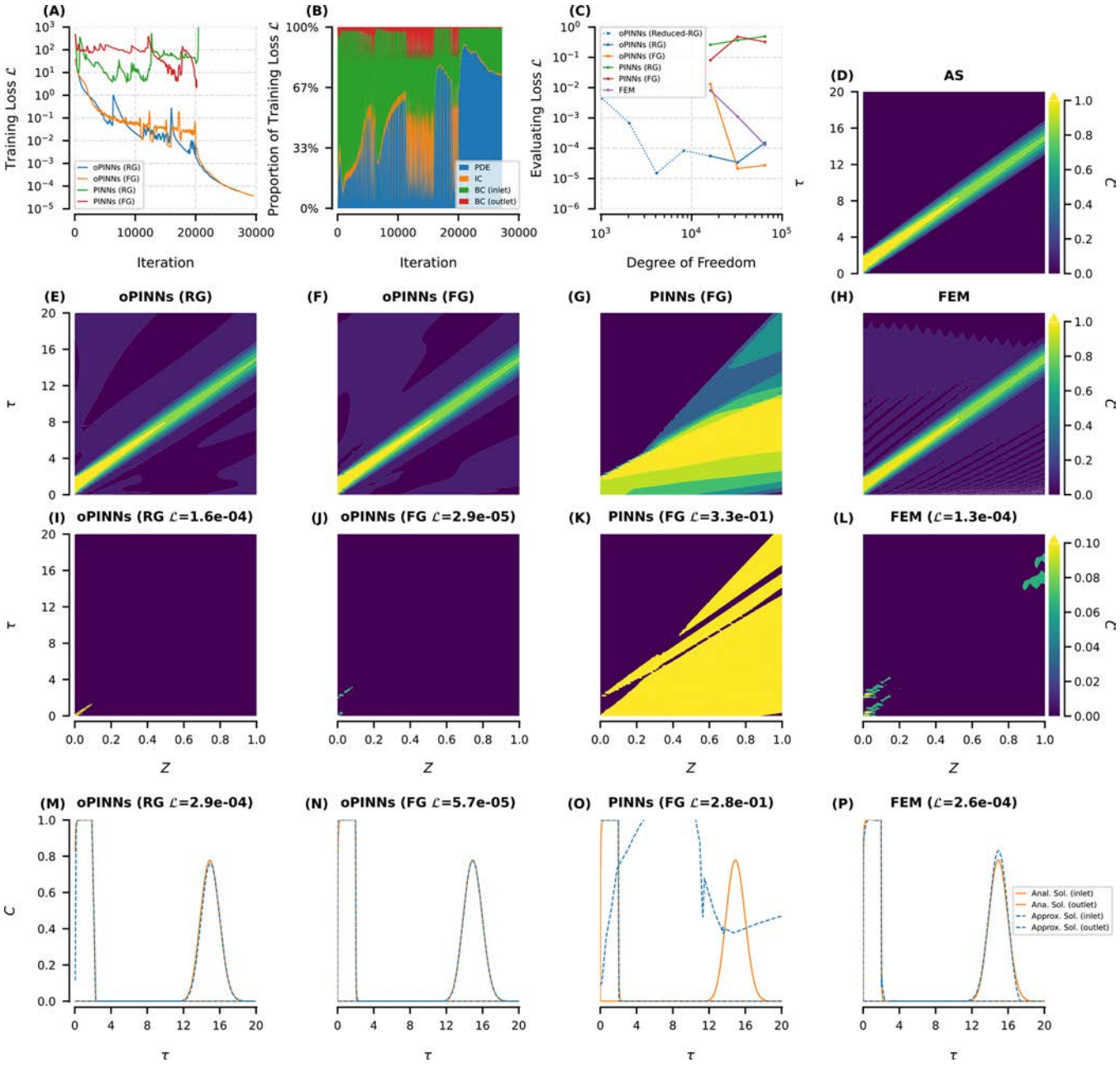

Figure 5. Pulse-injection experiments: losses during training processes (A), proportion of losses during training processes (B), convergence of approximate solutions (C), concentration distribution inside the column for analytical solution (D), oPINNs with RG mesh (E), oPINNs with FG mesh (F), PINNs with FG mesh (G), DG-FEM (H), absolute differences between the analytical solution and four approximate solutions (I–L), concentration distribution at the column inlet and outlet for the analytical solution and four approximate solutions (M–P).

mines the number of iterations based on the task load and calculates the average time cost.

4. RESULTS AND DISCUSSION

4.1. Hyperparameter Selection. The grid generated using uniform random sampling for hyperparameter search is shown in Figure 2A. The same grid was used to search the hyperparameters for both oPINNs and PINNs.

For pulse injection experiments, the hyperparameter search results for oPINNs are depicted in Figure 3K–T. Figure 3A quantitatively evaluates the importance of the five investigated hyperparameters by calculating the gradient of $\mathcal{L}$ with respect to each hyperparameter. The additional hyperparameter introduced, infinitesimal $o(C)$, is the least influential among the five, which suggests that introducing $o(C)$ does not significantly increase the complexity of the hyperparameter search. The model insensitivity to variations in this hyperparameter indicates strong robustness of oPINNs.

Figure 3A reveals that the number of neurons per layer n_l has the most significant impact. As observed in Figure 3K, increasing n_l effectively captures finer features in the samples, leading to lower training errors. However, when n_l is increased to 256, the excessive number of neurons results in a vastly expanded parameter space, making optimization extremely difficult. Figure 3A also demonstrates that the importance of learning rates follows n_l. Another structural parameter, the number of layers n_L, has a lesser impact.[38] Different activation functions exhibit significant performance differences in

https://doi.org/10.1021/acs.iecr.4c03744
Ind. Eng. Chem. Res. 2025, 64, 3168−3182

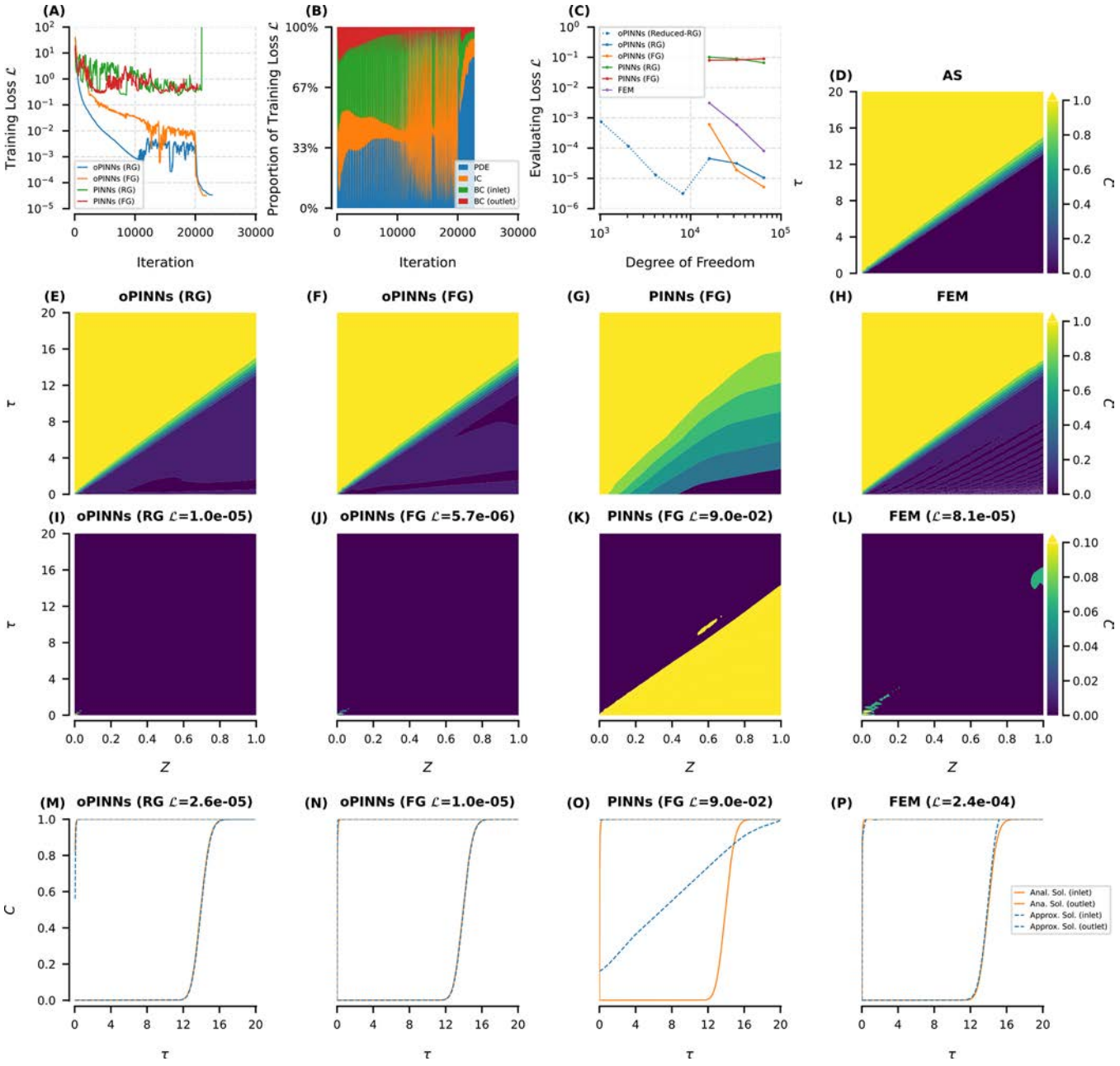

Figure 6. Breakthrough experiments: losses during training processes (A), proportion of losses during training processes (B), convergence of approximate solutions (C), concentration distribution inside the column for analytical solution (D), oPINNs with RG mesh (E), oPINNs with FG mesh (F), PINNs with FG mesh (G), DG-FEM (H), absolute differences between the analytical solution and four approximate solutions (I-L), concentration distribution at the column inlet and outlet for the analytical solution and four approximate solutions (M-P).

oPINNs, particularly the networks with the ReLU activation function.

Additionally, the empirical distribution function (EDF) curves for the 1512 hyperparameter search results of pulse injection experiments for oPINNs according to different learning rates are shown in Figure 3B. An EDF curve closer to the left means better model performance. Figure 3B shows that both excessively large and small learning rates degrade model performance, with the optimal learning rate at 10^{-3}.

For breakthrough experiments, the hyperparameter search results of oPINNs are illustrated in Figure 4K−T. As shown in Figure 4A, the importance of hyperparameters ranks from high to low as follows: n_L > activation function > $n_l \approx$ learning rate $\approx o(C)$. The optimal n_L ranges from 3 to 5, as indicated in Figure 4K.

Considering the hyperparameter selection results for both pulse injection and breakthrough experiments of oPINNs, the same hyperparameters was utilized: $n_L = 4$, $n_l = 64$, learning rate = 10^{-3}, Tanh activation function, $o(C) = 10^{-3}$. The total number of network parameters is 1153. None of these hyperparameters fall within the search boundaries, validating the rationality of the search space configuration. Once the infinitesimal is determined, the weight coefficients in oPINNs derived from first-principles are unique. This highlights a significant advantage of oPINNs: it minimizes the effort required to test various weight combinations. The corresponding EDF for these chosen hyperparameters is depicted in

https://doi.org/10.1021/acs.iecr.4c03744
Ind. Eng. Chem. Res. 2025, 64, 3168−3182

Table 3. Computational efficiency of oPINNs and DG-FEM for the forward problem of chromatographic models under varying sample sizes/grid densities

Method	Sample size/grid density	PI loss	BT loss	PI time cost/ms	BT time cost/ms
oPINNs (FG)	64640	2.74e-05	5.17e-06	9.34	8.25
oPINNs (FG)	32288	2.14e-05	1.89e-05	5.73	4.81
oPINNs (FG)	16128	1.30e-02	6.05e-04	5.08	4.09
oPINNs (RG)	65278	1.51e-04	1.05e-05	9.13	8.69
oPINNs (RG)	32578	3.40e-05	3.13e-05	5.79	4.79
oPINNs (RG)	16254	5.54e-05	4.52e-05	4.93	3.93
oPINNs (RG)	8200	8.31e-05	3.13e-06	4.28	3.90
oPINNs (RG)	4100	1.50e-05	1.29e-05	3.27	2.90
oPINNs (RG)	2050	6.67e-04	1.15e-04	3.51	3.07
oPINNs (RG)	1025	4.45e-03	7.36e-04	4.01	2.81
DG-FEM	64640, 3 order 16 elements	1.29e-04	8.08e-05	442	432
DG-FEM	32288, 3 order 8 elements	1.10e-03	5.96e-04	406	394
DG-FEM	16128, 3 order 4 elements	8.06e-03	3.09e-03	384	390

Figure 3B and Figure 4B. Under this hyperparameter combination, the loss for pulse injection experiments is 8.51 $\times 10^{-5}$ (better than 96.2% of combinations), and the loss for breakthrough experiments is 3.08 $\times 10^{-5}$ (better than 84.1% of combinations).

The hyperparameter search results for pulse injection and breakthrough experiments of PINNs are illustrated in Figure 3C−J and Figure 4C−J, respectively. The ordering of hyperparameter importance evaluation results in PINNs aligns with oPINNs, with the sole distinction that PINNs do not consider the hyperparameter $o(C)$. This observation indirectly suggests that the introduction of $o(C)$ in oPINNs does not lead to hyperparameter selection results radically different from PINNs, thus highlighting the robustness of oPINNs.

One notable difference from oPINNs observed in PINNs is the significant instability using ReLU as the activation function during pulse injection experiments. Both the worst and best performing combinations include the ReLU function, as depicted in Figure 3E−J and Figure 4E−J. The least effective (MSE > 1) hyperparameter combination consistently features ReLU activation, a learning rate of 10^{-2}, and n_l of 256. Across the hyperparameter results of oPINNs and PINNs, the combinations satisfying all three conditions consistently fail to yield satisfactory training outcomes. Zou et al.[36] also noted poor performance of ReLU activation in solving chromatographic models.

To simplify hyperparameter selection complexity, we strived to maintain consistency in the hyperparameter selection of PINNs with those of oPINNs, while excluding $o(C)$. Figure 3D and Figure 4D demonstrate the selected hyperparameters corresponding to EDF, with a loss of 2.99 $\times 10^{-1}$ for pulse injection experiments (superior to 28.6% of combinations) and 3.37 $\times 10^{-1}$ for breakthrough experiments (superior to 65.1% of combinations). The total number of network parameters in PINNs remains consistent with oPINNs.

4.2. Evaluation of Accuracy and Convergence. With the selected hyperparameter configurations, oPINNs and PINNs were trained using the FG (Figure 2B) and RG (Figure 2C) meshes, respectively. The training losses of the four models exhibit a continuously decreasing trend with increasing iterations, as shown in Figure 5A (pulse injection experiments) and Figure 6A (breakthrough experiments), indicating that the chosen learning rates were reasonable. Over a total of 30000 epochs, the proposed oPINNs consistently outperformed standard PINNs in terms of convergence in training loss. Standard PINNs with RG mesh exhibited divergence during L-BFGS optimization, a phenomenon absent in both RG and FG meshes with oPINNs.

Based on the optimal epochs obtained from training, we computed the concentration distributions inside the column for oPINNs (RG), oPINNs (FG), PINNs (FG), and DG-FEM, as illustrated in Figure 5E−H and Figure 6E−H. Comparison with analytical solutions (Figure 5D and Figure 6D) demonstrated that our proposed oPINNs can provide the best approximation to the analytical solutions. Standard PINNs showed significant deviation from the analytical solutions, while DG-FEM approximations exhibited slight numerical oscillations.

By computing the absolute differences between four approximate solutions (Figure 5E−H and Figure 6E−H) and the analytical solution (Figure 5D and Figure 6D), we obtained the evaluating errors of these four approximate solutions in concentration distributions of the column (Figure 5I−L and M−P as well as Figure 6I−L and M−P).

For the concentration distribution inside the column (Figure 5I−L and Figure 6I−L), at the same sample points, the evaluating error of oPINNs is approximately one order-of-magnitude lower than that of DG-FEM (2.9 $\times 10^{-5}$: 1.3 $\times 10^{-4}$ in pulse injection experiments for FG mesh and 1.0 $\times 10^{-5}$: 8.5 $\times 10^{-4}$ in breakthrough experiments for RG mesh). The error in DG-FEM primarily stems from the column inlet and outlet BCs (eqs 20 and 21). Both oPINNs and DG-FEM significantly outperform standard PINNs (by three to 4 orders of magnitude), which exhibit substantial errors in describing initial conditions (bottom boundary of the spatiotemporal coordinates in Figure 5K and Figure 6K).

Regarding the concentration distribution at the column inlet, all approximate solutions (excepting for standard PINNs) demonstrate consistency with the analytical solution, indicating effective minimization of $\mathcal{L}_{BC,in}$. At the column outlet (the most commonly measured signal in practical experiments), standard PINNs also exhibit significant errors, suggesting that $\mathcal{L}_{BC,out}$ was not adequately minimized for standard PINNs.[40] Furthermore, it could be observed that oPINNs perform better on FG mesh (Figure 2B) compared to RG mesh (Figure 2C), which exceeds our initial expectations. This suggests that using Jacobi polynomials to generate the mesh might be an effective approach for integrating traditional numerical methods with PINNs.

https://doi.org/10.1021/acs.iecr.4c03744
Ind. Eng. Chem. Res. 2025, 64, 3168−3182

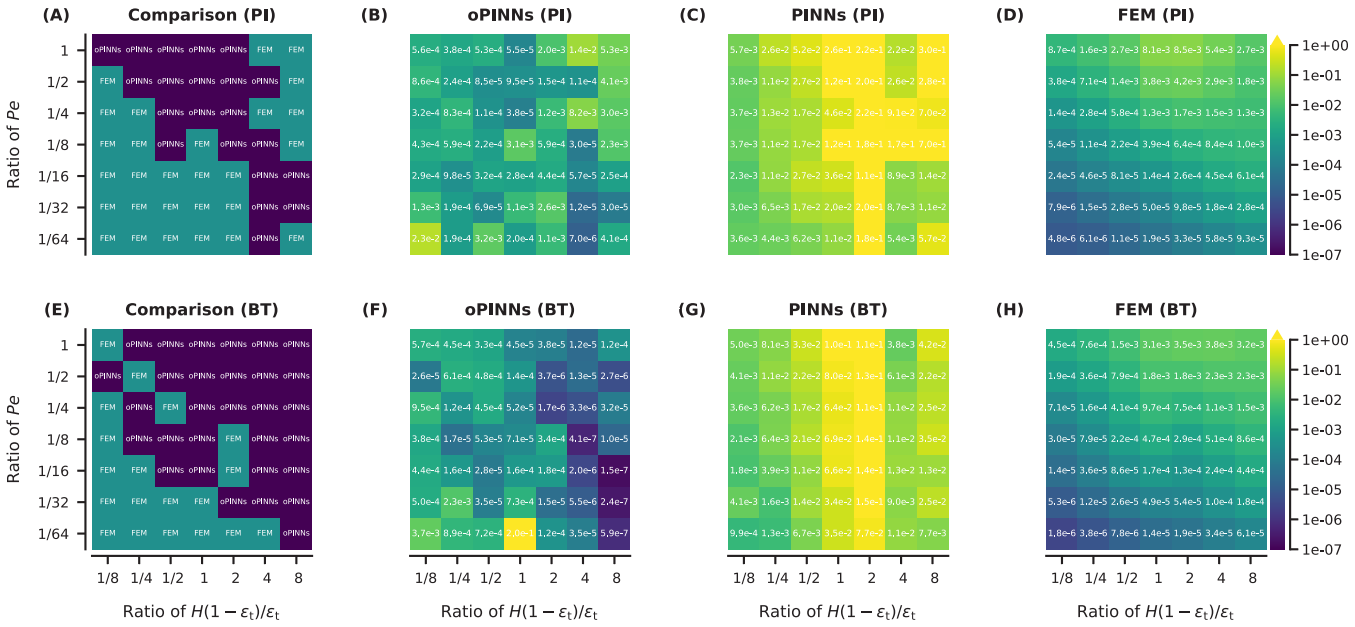

Figure 7. Optimal method for obtaining approximation solution of different model parameter ratios (A and E). Distribution of loss functions for oPINNs (B and F), PINNs (C and G), and FEM (D and H). First row: pulse injection experiments. Second row: breakthrough experiments.

Figure 5B and Figure 6B illustrate the proportion of training loss during the training process of oPINNs. The four loss terms exhibit a balanced distribution, each decreasing in proportion uniformly over 20,000 iterations of Adam optimization, while the L-BFGS optimizer effectively reduces errors associated with $\mathcal{L}_{BC,in}$. The model consistently tends to retain the smallest initialized contribution, $\mathcal{L}_{PDE}$, which starts with the smallest proportion and ends with the largest after training. Overall, the weights in oPINNs determined by order-of-magnitude analysis are reasonable, ensuring no single loss term dominates throughout the training process.

The four weights are specified as follows: $w_{IC} = 10^3$, $w_{BC,in} = 9.98 \times 10^{-1}$, $w_{BC,out} = 10^3$, and $w_{PDE} = 2.77 \times 10^1$. There exists a three-order-of-magnitude difference between the smallest weight ($w_{BC,in}$) and the largest weights (w_{IC} and $w_{BC,out}$). The equal weights in the unbiased PINNs results in $w_{BC,in}$ dominating the loss, explaining why PINNs only minimize $w_{BC,in}$ while diminishing optimization on other loss terms.

Figure 5C and Figure 6C evaluate the convergence of approximate solutions with varying sampling points, highlighting specific errors listed in Table 3. The theoretical convergence order of the third-order DG-FEM with central flux equals three. For pulse injection and breakthrough experiments, the experimental convergence order of DG-FEM is 3.00 and 2.62, respectively. In breakthrough experiments, the experimental convergence order of oPINNs is 3.43, indicating superior performance compared to DG-FEM and approaching the reported convergence order using Lax-Friedrichs flux.[54−56,62]

In Figure 5C and Figure 6C, it can be observed that increasing the sample points does not significantly improve the accuracy of oPINNs as expected, suggesting excessive computational resources are spent on additional sampling points. Therefore, we consider further reducing the sampling points to 1/8, 1/16, 1/32, 1/64 of DG-FEM and evaluate the errors. Figure 2D shows a 1/32 reduced-RG mesh. This reduction in sampling points does not excessively sacrifice the accuracy of oPINNs but significantly reduces computational resource consumption. This highlights the robustness of the proposed oPINNs in sampling point settings, whereas traditional DG-FEM heavily relies on grid refinement for accuracy improvement.

4.3. Evaluation of Robustness. The pulse injection and breakthrough experiments were conducted within the parameter space generated by varying ratios of $\frac{1-\varepsilon_t}{\varepsilon_t}H$ and Pe. The experiments involved oPINNs, standard PINNs, and DG-FEM, and the results are presented in grid plots as shown in Figure 7. Figure 7A summarizes the optimal method of different parameter ratios, where oPINNs and DG-FEM each achieve approximately half of the best solution, while standard PINNs notably underperform compared to the other two models. The weights for oPINNs were determined by these model parameters. This result confirms that within the specified range of model parameter variations, this weight determination significantly enhances the performance and robustness of oPINNs compared to standard PINNs.

In Figure 7B,F, the distribution of loss functions for oPINNs exhibits a complex relationship with the ratio of $\frac{1-\varepsilon_t}{\varepsilon_t}H$ and Pe. This complexity arises partly due to the dependency of oPINN weights on $\frac{1-\varepsilon_t}{\varepsilon_t}H$ and Pe, and potentially insufficient training iterations that may not fully exploit the oPINN capabilities. In contrast, as shown in Figure 7C,G, standard PINNs are insensitive to variations in Pe and converge to smaller losses at both ends of the range of $\frac{1-\varepsilon_t}{\varepsilon_t}H$. DG-FEM, as depicted in Figure 7D,H, demonstrates superior performance when dispersion dominates (smaller Pe).

This finding contrasts with He and Tartakovsky[63] observations in solving the two-dimensional convection-diffusion equation, where standard PINNs excel in scenarios with smaller Pe. We attribute this difference to our hyperparameters being chosen when the model parameter ratio was one, which may not be optimal for NNs after changing the ratios. Nevertheless, our results demonstrate that

https://doi.org/10.1021/acs.iecr.4c03744
Ind. Eng. Chem. Res. 2025, 64, 3168−3182

despite potentially suboptimal hyperparameter choices, oPINNs outperform traditional numerical methods significantly. However, as depicted in Figure 7A,E, particularly in the bottom-left region, oPINNs lose comparability with traditional methods when model parameters vary significantly from the selected hyperparameter point. This suggests that while the chosen hyperparameters exhibit robustness within a certain range of model parameter changes, a reevaluation of hyperparameter selection may be necessary when parameters vary beyond a certain extent.

4.4. Evaluation of Computational Efficiency. The computational efficiency of oPINNs and DG-FEM for the forward problem of linear chromatographic models under varying sample sizes/grid densities is summarized in Table 3.

DG-FEM takes approximately 400 ms, with a slight reduction in time as the grid sparsity increases. It is noteworthy that to ensure a fair comparison with oPINNs, we employed double-precision floating-point tensors in PyTorch for DG-FEM. This implementation includes a pure Python BDF time integrator, resulting in significant performance loss. Using NumPy implementation, solving time can be reduced to less than 100 ms, approaching performance levels reported for C++ implementations in literature.[54]

At the same grid density (sample size), oPINNs achieve higher computational accuracy compared to DG-FEM while improving computational speed by 50−75 times, with a calculation time of 4.09−9.34 ms per iteration. Further reducing sample sizes maintains comparable computational efficiency between oPINNs and DG-FEM, and oPINNs could achieve approximately 150 times faster computations than DG-FEM. This improvement is largely attributed to GPU acceleration. It should be noted that the computation times reported here are with automatic differentiation enabled. In practical forward problem inference using pretrained models, gradient information is unnecessary, allowing automatic differentiation to be disabled to conserve CPU and memory usage. With automatic differentiation disabled, oPINNs can achieve computation speeds over 1000 times faster than DG-FEM.

4.5. Discussion on Profound Implications of oPINNS. Our proposed oPINNs represent significant advancements to addresses the computational cost-accuracy trade-off inherent in traditional numerical methods. They can be significant advancements in solution accuracy (an order-of-magnitude improvement for accuracy with equivalent sample size or a 32-fold reduction in sample size for equivalent accuracy) and computational speed (a 1000-fold acceleration), relying on using order-of-magnitude analysis. Particularly, the introduction of infinitesimals establishes a perfect mapping between the chromatographic models and the loss function of NN.

Infinitesimals are most commonly associated with their pivotal role in calculus. Classical differentiation and integration are expressed as

$$f'(x) = \lim_{\Delta x \to 0} \frac{f(x + \Delta x) - f(x)}{\Delta x} \tag{37}$$

$$F(x) = \int f(x)\mathrm{d}x \tag{38}$$

where Δx and $\mathrm{d}x$ represent infinitesimals. Viewing calculus through the lens of NNs, for differentiation, the inputs comprise the original function $f(x)$ and the infinitesimal Δx, yielding the derivative $f'(x)$. Δx transforms $f(x)$ into $f'(x)$. For integration, the inputs involve the original function $f(x)$ and the infinitesimal $\mathrm{d}x$, yielding the integral $F(x)$. $\mathrm{d}x$ transforms $f(x)$ into $F(x)$. These infinitesimals Δx and $\mathrm{d}x$ serve as tools for scale transformations.

For oPINNs, the inputs are the original function $f(x)$ and the infinitesimal $o(x)$, yielding the approximation solution $F(x)$. $o(x)$ transforms $f(x)$ into $F(x)$. This transformation encompasses both integral and differential aspects, primarily focusing on differential forms for PDEs of chromatographic models. This understanding tightly integrates oPINNs with traditional calculus, providing mathematical meaning to solving PDEs using oPINNs.

Beyond mathematical interpretation, infinitesimal $o(x)$ can also be understood from a physical perspective. For instance, signifies the minimal change in concentration caused by adding a single solute molecule in a solution. This infinitesimal quantity should be equal to the reciprocal of Avogadro's constant.

If infinitesimals serve as a bridge connecting calculus to PINNs for solving PDEs, then order-of-magnitude analysis act as a lever for leveraging bioprocess dynamics with PINNs. Order-of-magnitude analysis allows comprehensive consideration of contribution of different dynamics to the loss function, thereby preventing domination by any single term. PDEs of bioprocess models can be transformed through rearrangement, multiplication, and division into various forms. For example, the column inlet BC in eq 20 can also be expressed by multiplying both sides by Pe:

$$-\frac{\partial C}{\partial Z}(0, \tau) + \mathrm{Pe}\cdot C(0, \tau) = \begin{cases} \mathrm{Pe} & 0 < \tau \le \tau_{\mathrm{inj}} \\ 0 & \tau > \tau_{\mathrm{inj}} \end{cases} \tag{39}$$

As a result, the corresponding loss term in Table 1 needs modification to

$$\mathcal{L}_{\mathrm{BC,in}} = \begin{cases} \left\| \frac{\partial C}{\partial Z}(0, \tau) - \mathrm{Pe}\cdot C(0, \tau) + \mathrm{Pe} \right\|_{L^2}^2 & 0 < \tau \le \tau_{\mathrm{inj}} \\ \left\| \frac{\partial C}{\partial Z}(0, \tau) - \mathrm{Pe}\cdot C(0, \tau) \right\|_{L^2}^2 & \tau > \tau_{\mathrm{inj}} \end{cases} \tag{40}$$

The reciprocal weight $w_{\mathrm{BC,in}}^{-1}$ determined by oPINNs method adjusts from $\frac{1}{\mathrm{Pe}} + 1$ to $\mathrm{Pe} + 1$, compensating for the impact of changes in the equation expression. Avoiding the need for reselecting and retraining network hyperparameters for different expression forms significantly enhances the practicality of oPINNs, a challenge that oPINNs can effectively address by seamlessly connecting the physical meaning of bioprocess models to the weights of loss terms.

4.6. Discussion on Prospects of oPINNS in Bioprocess Modeling. The proposed oPINNs imbue the loss function of PINNs with biological first-principles through order-of-magnitude analysis, significantly reducing barriers to integrating PINNs into hybrid modeling of bioprocesses.

For hyperparameter selection, oPINNs reduce all weight hyperparameters to a single infinitesimal. This reduction is particularly pronounced in multicomponent systems. For instance, in a ternary separation system, determining up to 12 weights would traditionally require evaluating $5^{12} = 2.44141$

https://doi.org/10.1021/acs.iecr.4c03744
Ind. Eng. Chem. Res. 2025, 64, 3168−3182

$\times 10^8$ combinations, rendering grid search impractical. By leveraging order-of-magnitude analysis, significant time savings can be achieved in hyperparameter search. For future studies using oPINNs, adopting a reasonable default value for the infinitesimal (e.g., 10^{-3}) can enhance model usability by minimizing the need for frequent adjustments and simplifying the tuning process.

The proposed oPINNs demonstrate robustness in both weight determination and hyperparameter selection when the parameters of chromatographic models vary within a certain range. This robustness allows oPINNs to extend from solving individual PDEs to solving multiple PDEs (with model parameter variations), thereby enhancing their practical applicability. Future exploration will focus on solving series chromatographic models.

The comparison of computation speed using identical hardware, implementation methods, and computational precision is fair. The GPU accelerator plays a pivotal role in achieving millisecond-scale simulation of chromatography processes with oPINNs, leveraging parallel computing across thousands of CUDA cores. With GPU accelerators, physics-based deep learning lays the foundation for future real-time applications such as process control and digital twin development.[64] For instance, developing a real-time digital twin for chromatography, combined with soft sensors and GPU edge computing inference,[65−68] enables monitoring, analysis, optimization, prediction, and control of the chromatography process based on real-time models.[69] This can achieve a bidirectional link between the physical and virtual worlds.

Efficiency of physics-based deep learning solvers like oPINNs can be further enhanced by optimizing network structures.[70] The achieved 1000-fold acceleration in computational speed in this study may not represent the upper limit. For instance, Li et al.[71] reduced the solution time of Navier−Stokes equations from 18 h to 5 ms using physics-based deep learning, achieving a speedup of 6.48×10^7 times over traditional numerical methods. This suggests that oPINNs could offer even greater computational efficiency advantages in handling complex models.[35] Our future work aims to apply PINNs to develop the more sophisticated chromatographic hybrid models based on general rate models and nonlinear isotherm models.

5. CONCLUSIONS

This work proposed a novel physics-based deep learning method by integrating of order-of-magnitude analysis into PINNs (oPINNs). oPINNs imbued the loss function with biological first-principles, significantly reducing barriers to integrating PINNs into hybrid modeling of bioprocesses. In comparison to standard PINNs and numerical methods for solving the forward problem of linear chromatographic models, oPINNs could achieve notable improvements: an order-of-magnitude enhancement in accuracy with an equivalent sample size, or a 32-fold reduction in sample size for equivalent accuracy, along with a 1000-fold acceleration in computational speed for millisecond-scale simulation. These enhancements effectively address the computational cost-accuracy trade-off inherent in traditional numerical methods. Moreover, oPINNs showed exceptional robustness in weight determination and hyperparameter selection amidst variations in chromatographic model parameters. In summary, oPINNs represent a significant advancement in integrating physics-based deep learning into hybrid modeling of bioprocesses, particularly for developing real-time digital twins.

■ ASSOCIATED CONTENT

Data Availability Statement

Data will be made available on request.

■ AUTHOR INFORMATION

Corresponding Author

Dong-Qiang Lin − *Key Laboratory of Biomass Chemical Engineering of Ministry of Education, Zhejiang Key Laboratory of Smart Biomaterials, College of Chemical and Biological Engineering, Zhejiang University, Hangzhou 310058, China;* orcid.org/0000-0002-0504-8391; Email: lindq@zju.edu.cn

Authors

Yu-Cheng Chen − *Key Laboratory of Biomass Chemical Engineering of Ministry of Education, Zhejiang Key Laboratory of Smart Biomaterials, College of Chemical and Biological Engineering, Zhejiang University, Hangzhou 310058, China*

Shan-Jing Yao − *Key Laboratory of Biomass Chemical Engineering of Ministry of Education, Zhejiang Key Laboratory of Smart Biomaterials, College of Chemical and Biological Engineering, Zhejiang University, Hangzhou 310058, China;* orcid.org/0000-0003-3199-3044

Complete contact information is available at: https://pubs.acs.org/10.1021/acs.iecr.4c03744

Notes

The authors declare no competing financial interest.

■ ACKNOWLEDGMENTS

This work was supported by the Zhejiang Key Science and Technology Project (2023C03116), National Natural Science Foundation of China (22078286), Huadong Medicine Joint Funds of the Zhejiang Provincial Natural Science Foundation of China (LHDMZ24B060001), and China Scholarship Council (CSC, no. 202306320355). The authors would also like to thank the State Key Laboratory of Fire Science, University of Science and Technology of China, and the Zhejiang University Information Technology Center for the cloud computing service.

■ REFERENCES

(1) Mahanty, B. Hybrid modeling in bioprocess dynamics: Structural variabilities, implementation strategies, and practical challenges. *Biotechnol. Bioeng.* **2023**, *120* (8), 2072−2091.

(2) Roush, D.; Asthagiri, D.; Babi, D. K.; Benner, S.; Bilodeau, C.; Carta, G.; Ernst, P.; Fedesco, M.; Fitzgibbon, S.; Flamm, M.; et al. Toward in silico CMC: An industrial collaborative approach to model-based process development. *Biotechnol. Bioeng.* **2020**, *117* (12), 3986−4000.

(3) Jungbauer, A.; Ferreira, G.; Butler, M.; D'Costa, S.; Brower, K.; Rayat, A.; Willson, R. Status and future developments for downstream processing of biological products. *Biotechnol. Bioeng.* **2024**, *121* (8), 2524−2541.

(4) Wittkopp, F.; Welsh, J.; Todd, R.; Staby, A.; Roush, D.; Lyall, J.; Karkov, S.; Hunt, S.; Griesbach, J.; Bertran, M.-O.; et al. Current state of implementation of in silico tools in the biopharmaceutical industry—Proceedings of the 5th modeling workshop. *Biotechnol. Bioeng.* **2024**, *121* (9), 2952−2973.

(5) Bradley, W.; Kim, J.; Kilwein, Z.; Blakely, L.; Eydenberg, M.; Jalvin, J.; Laird, C.; Boukouvala, F. Perspectives on the integration between first-principles and data-driven modeling. *Comput. Chem. Eng.* **2022**, *166*, No. 107898.
(6) Chen, Y.; Ierapetritou, M. A framework of hybrid model development with identification of plant-model mismatch. *AIChE J.* **2020**, *66* (10), No. e16996.
(7) Ding, C. Y.; Gerberich, C.; Ierapetritou, M. Hybrid model development for parameter estimation and process optimization of hydrophobic interaction chromatography. *J. Chromatogr. A* **2023**, *1703*, No. 464113.
(8) Narayanan, H.; Luna, M.; Sokolov, M.; Butté, A.; Morbidelli, M. Hybrid Models Based on Machine Learning and an Increasing Degree of Process Knowledge: Application to Cell Culture Processes. *Ind. Eng. Chem. Res.* **2022**, *61* (25), 8658−8672.
(9) Narayanan, H.; Sponchioni, M.; Morbidelli, M. Integration and digitalization in the manufacturing of therapeutic proteins. *Chem. Eng. Sci.* **2022**, *248*, No. 117159.
(10) Koksal, E. S.; Asrav, T.; Esenboga, E. E.; Cosgun, A.; Kusoglu, G.; Aydin, E. Physics-informed and data-driven modeling of an industrial wastewater treatment plant with actual validation. *Comput. Chem. Eng.* **2024**, *189*, No. 108801.
(11) Chen, Y.-C.; Zhong, X.-Z.; Shi, C.; Chen, R.; Sponchioni, M.; Yao, S.-J.; Lin, D.-Q. Mechanistic modeling of anti-Langmuirian to Langmuirian behavior of Fc-fusion proteins in cation exchange chromatography. *J. Chromatogr. A* **2025**, *1741*, No. 465602.
(12) Chen, Y.-C.; Chen, X.-Y.; Lin, Z.-Y.; Yao, S.-J.; Lin, D.-Q. Practical teaching of modeling tools for ion-exchange chromatography: A case study. *J. Chem. Educ.* **2023**, *100* (10), 3888−3896.
(13) Chen, Y.-C.; Yao, S.-J.; Lin, D.-Q. Enhancing thermodynamic consistency: Clarification on the application of asymmetric activity model in multi-component chromatographic separation. *J. Chromatogr. A* **2024**, *1731*, No. 465156.
(14) Chen, Y.-C.; Lu, H. L.; Wang, R. Z.; Sun, G.; Zhang, X. Q.; Liang, J. Q.; Jungbauer, A.; Yao, S. J.; Lin, D. Q. Standardized approach for accurate and reliable model development of ion-exchange chromatography based on parameter-by-parameter method and consideration of extra-column effects. *Biotechnol. J.* **2024**, *19* (3), 2300687.
(15) Chen, Z.; Liu, Y.; Sun, H. Physics-informed learning of governing equations from scarce data. *Nat. Commun.* **2021**, *12* (1), 6136.
(16) Karniadakis, G. E.; Kevrekidis, I. G.; Lu, L.; Perdikaris, P.; Wang, S. F.; Yang, L. Physics-informed machine learning. *Nat. Rev. Phys.* **2021**, *3* (6), 422−440.
(17) Kharazmi, E.; Cai, M.; Zheng, X. N.; Zhang, Z.; Lin, G.; Karniadakis, G. E. Identifiability and predictability of integer- and fractional-order epidemiological models using physics-informed neural networks. *Nat. Comput. Sci.* **2021**, *1* (11), 744−753.
(18) Borate, P.; Rivière, J.; Marone, C.; Mali, A.; Kifer, D.; Shokouhi, P. Using a physics-informed neural network and fault zone acoustic monitoring to predict lab earthquakes. *Nat. Commun.* **2023**, *14* (1), 3693.
(19) Shen, C. P.; Appling, A. P.; Gentine, P.; Bandai, T.; Gupta, H.; Tartakovsky, A.; Baity-Jesi, M.; Fenicia, F.; Kifer, D.; Li, L.; et al. Differentiable modelling to unify machine learning and physical models for geosciences. *Nat. Rev. Earth Environ.* **2023**, *4* (8), 552−567.
(20) Wang, F. J.; Zhai, Z.; Zhao, Z. B.; Di, Y.; Chen, X. F. Physics-informed neural network for lithium-ion battery degradation stable modeling and prognosis. *Nat. Commun.* **2024**, *15* (1), 4332.
(21) Lu, Z. B.; Li, Y. M.; He, C.; Ren, J. Z.; Yu, H. S.; Zhang, B. J.; Chen, Q. L. Multi-objective inverse design of finned heat sink system with physics-informed neural networks. *Comput. Chem. Eng.* **2024**, *180*, No. 108500.
(22) Zhu, L. T.; Chen, X. Z.; Ouyang, B.; Yan, W. C.; Lei, H.; Chen, Z.; Luo, Z. H. Review of Machine Learning for Hydrodynamics, Transport, and Reactions in Multiphase Flows and Reactors. *Ind. Eng. Chem. Res.* **2022**, *61* (28), 9901−9949.
(23) Zheng, Y. Z.; Wu, Z. Physics-Informed Online Machine Learning and Predictive Control of Nonlinear Processes with Parameter Uncertainty. *Ind. Eng. Chem. Res.* **2023**, *62* (6), 2804−2818.
(24) Wu, Z. Y.; Wang, H.; He, C.; Zhang, B. J.; Xu, T.; Chen, Q. L. The Application of Physics-Informed Machine Learning in Multiphysics Modeling in Chemical Engineering. *Ind. Eng. Chem. Res.* **2023**, *62* (44), 18178−18204.
(25) Sorourifar, F.; Peng, Y.; Castillo, I.; Bui, L.; Venegas, J.; Paulson, J. A. Physics-Enhanced Neural Ordinary Differential Equations: Application to Industrial Chemical Reaction Systems. *Ind. Eng. Chem. Res.* **2023**, *62* (38), 15563−15577.
(26) Moayedi, F.; Chandrasekar, A.; Rasmussen, S.; Sarna, S.; Corbett, B.; Mhaskar, P. Physics-Informed Neural Networks for Process Systems: Handling Plant-Model Mismatch. *Ind. Eng. Chem. Res.* **2024**, *63* (31), 13650−13659.
(27) de Rezende Faria, R.; Capron, B. D. O.; Secchi, A. R.; de Souza, M. B. Gas-Lift Optimization Using Physics-Informed Deep Reinforcement Learning. *Ind. Eng. Chem. Res.* **2024**, *63* (32), 14199−14210.
(28) Espinel-Ríos, S.; Avalos, J. L. Hybrid Physics-Informed Metabolic Cybergenetics: Process Rates Augmented with Machine-Learning Surrogates Informed by Flux Balance Analysis. *Ind. Eng. Chem. Res.* **2024**, *63* (15), 6685−6700.
(29) Makrygiorgos, G.; Berliner, A. J.; Shi, F.; Clark, D. S.; Arkin, A. P.; Mesbah, A. Data-driven flow-map models for data-efficient discovery of dynamics and fast uncertainty quantification of biological and biochemical systems. *Biotechnol. Bioeng.* **2023**, *120* (3), 803−818.
(30) Mowbray, M. R.; Wu, C.; Rogers, A. W.; Rio-Chanona, E. A. D.; Zhang, D. A reinforcement learning-based hybrid modeling framework for bioprocess kinetics identification. *Biotechnol. Bioeng.* **2023**, *120* (1), 154−168.
(31) Rydal, T.; Frandsen, J.; Nadal-Rey, G.; Albaek, M. O.; Ramin, P. Bringing a scalable adaptive hybrid modeling framework closer to industrial use: Application on a multiscale fungal fermentation. *Biotechnol. Bioeng.* **2024**, *121* (5), 1609−1625.
(32) Mouellef, M.; Vetter, F. L.; Strube, J. Benefits and limitations of artificial neural networks in process chromatography design and operation. *Processes* **2023**, *11* (4), 1115.
(33) Yang, S.; Fahey, W.; Truccollo, B.; Browning, J.; Kamyar, R.; Cao, H. Hybrid Modeling of Fed-Batch Cell Culture Using Physics-Informed Neural Network. *Ind. Eng. Chem. Res.* **2024**, *63* (39), 16833−16846.
(34) Santana, V. V.; Gama, M. S.; Loureiro, J. M.; Rodrigues, A. E.; Ribeiro, A. M.; Tavares, F. W.; Barreto, A. G.; Nogueira, I. B. R. A first approach towards adsorption-oriented physics-informed neural networks: Monoclonal antibody adsorption performance on an ion-exchange column as a case study. *Chemengineering* **2022**, *6* (2), 21.
(35) Tang, S.-Y.; Yuan, Y.-H.; Chen, Y.-C.; Yao, S.-J.; Wang, Y.; Lin, D.-Q. Physics-informed neural networks to solve lumped kinetic model for chromatography process. *J. Chromatogr. A* **2023**, *1708*, No. 464346.
(36) Zou, T.; Yajima, T.; Kawajiri, Y. A parameter estimation method for chromatographic separation process based on physics-informed neural network. *J. Chromatogr. A* **2024**, *1730*, No. 465077.
(37) Söderström, P. *Physics-informed neural networks for liquid chromatography*. MSc Thesis, Umea University, 2022. https://urn.kb.se/resolve?urn=urn:nbn:se:umu:diva-196783.
(38) Subraveti, S. G.; Li, Z.; Prasad, V.; Rajendran, A. Can a computer "learn" nonlinear chromatography?: Physics-based deep neural networks for simulation and optimization of chromatographic processes. *J. Chromatogr. A* **2022**, *1672*, No. 463037.
(39) Subraveti, S. G.; Li, Z.; Prasad, V.; Rajendran, A. Physics-based neural networks for simulation and synthesis of cyclic adsorption processes. *Ind. Eng. Chem. Res.* **2022**, *61* (11), 4095−4113.
(40) Subraveti, S. G.; Li, Z.; Prasad, V.; Rajendran, A. Can a Computer "Learn" Nonlinear Chromatography?: Experimental Validation of Physics-Based Deep Neural Networks for the Simulation of Chromatographic Processes. *Ind. Eng. Chem. Res.* **2023**, *62* (14), 5929−5944.

https://doi.org/10.1021/acs.iecr.4c03744
Ind. Eng. Chem. Res. 2025, 64, 3168−3182

(41) Thuerey, N.; Holl, P.; Mueller, M.; Schnell, P.; Trost, F.; Um, K.Physics-based Deep Learning; *arXiv* **2021**. DOI: .
(42) Montévil, M.; Soto, A. M.Modeling Organogenesis from Biological First Principles. In *Organization in Biology*, Mossio, M., Ed.; Springer International Publishing, 2024; pp 263−283.
(43) Li, P.; Yu, J. G.; Xiu, G. H.; Rodrigues, A. E. A Strategy for Tailored Design of Efficient and Low-Pressure Drop Packed Column Chromatography. *AIChE J.* **2010**, *56* (12), 3091−3098.
(44) Khelifa, N. B.; Alloui, Z.; Beji, H.; Vasseur, P. Natural convection in a vertical porous cavity filled with a non-newtonian binary fluid. *AIChE J.* **2012**, *58* (6), 1704−1716.
(45) Jungbauer, A.; Satzer, P.; Duerauer, A.; Azevedo, A.; Aires-Barros, R.; Nilsson, B.; Farid, S.; Goldrick, S.; Ottens, M.; Sponchioni, M.; et al. Continuous downstream processing. *Sep. Purif. Technol.* **2024**, *338*, No. 126439.
(46) Van Genuchten, M. T. Analytical solutions for chemical transport with simultaneous adsorption, zero-order production and first-order decay. *J. Hydrol.* **1981**, *49* (3), 213−233.
(47) Qamar, S.; Abbasi, J. N.; Javeed, S.; Shah, M.; Khan, F. U.; Seidel-Morgenstern, A. Analytical solutions and moment analysis of chromatographic models for rectangular pulse injections. *J. Chromatogr. A* **2013**, *1315*, 92−106.
(48) Chen, Y.-C.; Recanati, G.; De Mathia, F.; Lin, D. Q.; Jungbauer, A. Residence time distribution in continuous virus filtration. *Biotechnol. Bioeng.* **2024**, *121* (6), 1876−1888.
(49) Lin, D.-Q.; Chen, Y.-C.; Chen, X.-Y.; Yao, S.-J. Exploration and Practice of Online−Offline Blended Teaching in Process Simulation Courses. *J. Chem. Educ.* **2024**, *101* (5), 1966−1973.
(50) Qu, Y.; Baker, I.; Black, J.; Fabri, L.; Gras, S. L.; Lenhoff, A. M.; Kentish, S. E. Application of mechanistic modelling in membrane and fiber chromatography for purification of biotherapeutics — A review. *J. Chromatogr. A* **2024**, *1716*, No. 464588.
(51) Altern, S. H.; Lyall, J. Y.; Welsh, J. P.; Burgess, S.; Kumar, V.; Williams, C.; Lenhoff, A. M.; Cramer, S. M. High-throughput in silico workflow for optimization and characterization of multimodal chromatographic processes. *Biotechnol. Prog.* **2024**, *40* (6), No. e3483.
(52) Eslami, T.; Jungbauer, A. Control strategy for biopharmaceutical production by model predictive control. *Biotechnol. Prog.* **2024**, *40* (2), No. e3426.
(53) Gusmao, G. S.; Medford, A. J. Maximum-likelihood estimators in physics-informed neural networks for high-dimensional inverse problems. *Comput. Chem. Eng.* **2024**, *181*, No. 108547.
(54) Breuer, J. M.; Leweke, S.; Schmölder, J.; Gassner, G.; von Lieres, E. Spatial discontinuous Galerkin spectral element method for a family of chromatography models in CADET. *Comput. Chem. Eng.* **2023**, *177*, No. 108340.
(55) Qamar, S.; Perveen, S.; Tabib, K.; Rehman, N.; Rehman, F. Discontinuous Galerkin finite element method for solving non-linear model of gradient elution chromatography. *Adsorption* **2024**, *30*, 1161−1174.
(56) Meyer, K.; Søes Ibsen, M.; Vetter-Joss, L.; Broberg Hansen, E.; Abildskov, J. Industrial ion-exchange chromatography development using discontinuous Galerkin methods coupled with forward sensitivity analysis. *J. Chromatogr. A* **2023**, *1689*, No. 463741.
(57) Chen, Y.-C.; Yao, S.-J.; Lin, D.-Q. Parameter-by-parameter method for steric mass action model of ion exchange chromatography: Theoretical considerations and experimental verification. *J. Chromatogr. A* **2022**, *1680*, No. 463418.
(58) Chen, Y.-C.; Yao, S.-J.; Lin, D.-Q. Parameter-by-parameter method for steric mass action model of ion exchange chromatography: Simplified estimation for steric shielding factor. *J. Chromatogr. A* **2023**, *1687*, No. 463655.
(59) Chen, H.; Flores, G. E. C.; Li, C. Physics-informed neural networks with hard linear equality constraints. *Comput. Chem. Eng.* **2024**, *189*, No. 108764.
(60) Asrav, T.; Aydin, E. Physics-informed recurrent neural networks and hyper-parameter optimization for dynamic process systems. *Comput. Chem. Eng.* **2023**, *173*, No. 108195.
(61) Seidel-Morgenstern, A. Modeling of chromatographic processes. In *Preparative Chromatography*, 3 ed.; Schmidt-Traub, H.; Schulte, M.; Seidel-Morgenstern, A., Eds.; Wiley-CH Verlag GmbH & Co. KGaA, 2020; pp 311−354.
(62) Khan, A.; Perveen, S.; Qamar, S. Discontinuous Galerkin Scheme for Solving a Lumped Kinetic Model of Non-isothermal Liquid Chromatography with Bi-Langmuir Isotherms. *Ind. Eng. Chem. Res.* **2021**, *60* (34), 12592−12601.
(63) He, Q. Z.; Tartakovsky, A. M. Physics-informed neural network method for forward and backward advection-dispersion equations. *Water Resour. Res.* **2021**, *57* (7), e2020WR029479.
(64) Chopda, V.; Gyorgypal, A.; Yang, O.; Singh, R.; Ramachandran, R.; Zhang, H. R.; Tsilomelekis, G.; Chundawat, S. P. S.; Ierapetritou, M. G. Recent advances in integrated process analytical techniques, modeling, and control strategies to enable continuous biomanufacturing of monoclonal antibodies. *J. Chem. Technol. Biotechnol.* **2022**, *97* (9), 2317−2335.
(65) Schiemer, R.; Weggen, J. T.; Schmitt, K. M.; Hubbuch, J. An adaptive soft-sensor for advanced real-time monitoring of an antibody-drug conjugation reaction. *Biotechnol. Bioeng.* **2023**, *120* (7), 1914−1928.
(66) Tiwari, A.; Masampally, V. S.; Agarwal, A.; Rathore, A. S. Digital twin of a continuous chromatography process for mAb purification: Design and model-based control. *Biotechnol. Bioeng.* **2023**, *120* (3), 748−766.
(67) Silva, T. C.; Eppink, M.; Ottens, M. Digital twin in high throughput chromatographic process development for monoclonal antibodies. *J. Chromatogr. A* **2024**, *1717*, No. 464672.
(68) Zobel-Roos, S.; Vetter, F.; Scheps, D.; Pfeiffer, M.; Gunne, M.; Boscheinen, O.; Strube, J. Digital Twin Based Design and Experimental Validation of a Continuous Peptide Polishing Step. *Processes* **2023**, *11* (5), 1401.
(69) Wang, J.; Chen, J.; Studts, J.; Wang, G. In-line product quality monitoring during biopharmaceutical manufacturing using computational Raman spectroscopy. *mAbs* **2023**, *15* (1), 2220149.
(70) Koksal, E. S.; Aydin, E. Physics Informed Piecewise Linear Neural Networks for Process Optimization. *Comput. Chem. Eng.* **2023**, *174*, No. 108244.
(71) Li, Z.; Kovachki, N.; Azizzadenesheli, K.; Liu, B.; Bhattacharya, K.; Stuart, A.; Anandkumar, A. Fourier neural operator for parametric partial differential equations. *arXiv* **2020**, DOI: .

https://doi.org/10.1021/acs.iecr.4c03744
Ind. Eng. Chem. Res. 2025, 64, 3168−3182